IEEE Photonics Journal
An IEEE Photonics Society Publication

Open Access

VROHI: Visibility Recovery for Outdoor Hazy Image in Scattering Media

Volume 12, Number 6, December 2020

Mingye Ju
Can Ding, *Member, IEEE*
Y. Jay Guo, *Fellow, IEEE*

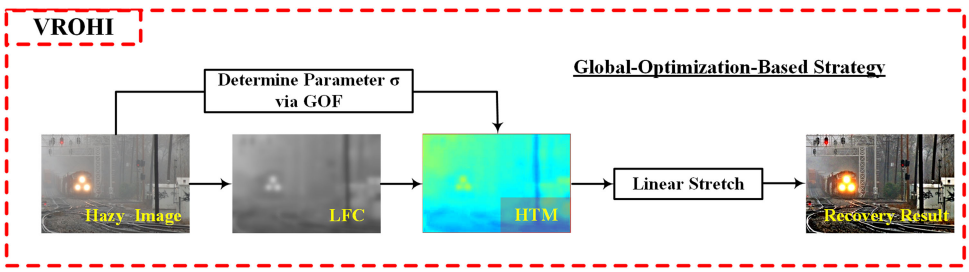

DOI: 10.1109/JPHOT.2020.3036873

IEEE photonics SOCIETY
IEEE

VROHI: Visibility Recovery for Outdoor Hazy Image in Scattering Media

Mingye Ju,[1,2] **Can Ding**,[2] ***Member, IEEE***,
and Y. Jay Guo,[2] ***Fellow, IEEE***

[1]School of Internet of Things, Nanjing University of Posts and Telecommunications, Nanjing 210000, China
[2]Global Big Data Technologies Centre, University of Technology Sydney, Ultimo, NSW 2007, Australia

DOI:10.1109/JPHOT.2020.3036873

Manuscript received September 25, 2020; revised November 2, 2020; accepted November 4, 2020. Date of publication November 10, 2020; date of current version December 4, 2020. This work was supported in part by the National Natural Science Foundation of China (61902198), in part by the Natural Science Foundation of Jiangsu Province (BK20190730), and in part by Research Fund of Nanjing University of Posts and Telecommunications (NY219135). Corresponding author: Can Ding (email: Can.Ding@uts.edu.au.)

Abstract: Additive haze model (AHM), due to its high simplicity, has a potential to increase the efficiency of the restoration procedure of images degraded by scattering media. However, AHM is designed for hazy remote sensing data and is not suitable to be used on outdoor images. In this paper, according to the low-frequency feature (LFC) of haze, AHM is modified via gamma correction technique to make it suitable for modeling outdoor images. Benefitting from the modified AHM (MAHM), a simple yet effective method called VROHI is proposed to enhance the visibility of an outdoor hazy image. In specific, a low complexity LFC extraction method is designed by utilizing characteristic of the discrete cosine transform. Subsequently, by constructing the linear function of unknown parameters and imposing the saturation prior on MAHM, the image dehazing problem can be derived into a global optimization function. Experiments reveal that the proposed VROHI is superior to the other state-of-the-art techniques in terms of both the processing efficiency and recovery quality.

Index Terms: Additive haze model, global optimization dehazing, haze thickness map, low-frequency component, propagation and scattering.

1. Introduction

Images captured under hazy weather conditions may suffer from contrast reduction and inconsistent colors. This is due to the reflected light from objects can be scattered, refracted, and absorbed by the particles suspended in atmosphere, e.g., water vapor, fog, sand, dust, or smoke. This interference not only reduces visual quality of observed images, but also affects the accuracy of image feature extraction, thereby leading to some errors in computer vision systems. Therefore, image haze removal is crucial for many applications that need high-quality inputs.

Early works [1], [2] directly employed the traditional image enhancement techniques to stretch the contrast of hazy images, but the visual quality of recovered results is limited. The main reason is that traditional methods only focus on increasing the contrast in degraded scenes rather than removing the haze theoretically. Another kind of solutions advocated in [3]–[6] is able to generate a better result by introducing additional information. For example, Kopf *et al.* [3] utilized the given

geo-referenced digital terrain to remove the haze cover in images. Li *et al.* [4] developed a simple pseudo-polarimetric dehazing method for dense haze removal using polarization property. According to different atmospheric properties, Narasimhan *et al.* [5] used two given images to derive the scene depth and other parameters that are required to recover the image. Although high-quality dehazing results can be obtained by these methods, they require high cost prerequisites and thus limiting their practicability for many applications.

Compared to the aforementioned two kinds of image dehazing methods, recently published works [7]–[25] have achieved more promising performances. In these technologies, the haze-relevant information is extracted from only one input image and processed by complex mathematical tools to obtain a recovery result. In general, they can be further divided into three categories:

1) The first category is atmosphere scattering model (ASM) based methods [7]–[16]. These methods are based on ASM [5], but they also utilize latent prior knowledge to constrain ASM. In general, these methods are capable of producing reliable results for most cases. However, they are not able to handle all practical situations and exhibit some limitations when dealing with certain kinds of images. For example, He *et al.* [7] proposed to use dark channel prior (DCP) to estimate the transmission of input image before haze-free result can be restored via ASM. The performance of this method is mostly promising, but it cannot well handle the regions where scene objects are inherently similar to the atmospheric light. In [8], Bi *et al.* introduced a brightness map to improve the recovery quality of DCP method. Ref. [9] proposed a quadtree theory to locate the atmospheric light, and estimated the transmission by combining coefficient modification and DCP. In [10], before applying ASM, the optimal transmission was obtained by assuming that each local patch can be linearly represented by a dictionary. This prior is very reliable and can lead to good recovered results, whereas the white regions containing texture details always have slight color errors. In [11], Wang *et al.* achieved haze removal using a linear transformation that exists in the minimum channel between hazy input and haze-free image. The main advantage of this method is its low complexity, yet the fixed control factor involved in this method leads to the dim scene content. Based on a key assumption that an outdoor image contains approximated colors or repeated patches, non-local strategies [12]–[14] were developed to exclude the haze shroud in images. Unfortunately, as the hazy level increases, these methods may reduce their dehazing performance since the classification accuracy of colors or patches would be degraded.

2) The second category is multi-scale-fusion-based methods [17]–[19]. The strategy of these methods is to generate two or more images by processing an input image with traditional enhancement techniques, then to merge these processed images to get a better restoration result. Typically, Ancuti and Ancuti [17] developed a visibility recovery method based on Laplacian pyramid representation. In this work, an input image was firstly preprocessed by white balance and contrast enhancement, leading to two images with different properties. Then the two images were blended to a haze-free result by using a Laplacian pyramid representation. To achieve a better recovery quality, Choi *et al.* [18] introduced more image features to participate the fusion process. Later in [19], another fusion-based dehazing technique was designed by simply finding contrasted/saturated regions from some artificially under-exposed versions of hazy input. The main advantage of multi-fusion-based methods is the high implementation efficiency, but their performance is deteriorated when dealing with the dark regions in hazy image. This is due to the fact that the severe dark parts of the preprocessed images are usually misjudged as the haze-free scenes.

3) The third category is deep-learning-based methods [20]–[25]. Benefitting from the development of deep learning (DL) theory, haze removal can be realized by merging or learning several haze-relevant features with the DL framework. For instance, a convolutional neural network (CNN) based dehazing system, called DehazeNet, was proposed in [20] by fully utilizing the existing image priors. In subsequence, a multi-scale CNN (MSCNN) was proposed in [21] to achieve a better recovery quality by learning more useful features. However, these approaches need to introduce guided filter or fine-scale net to repair the artifacts in the estimated rough transmission. To remedy this, Li *et al.* [22] built a dehazing model called All-in-One Dehazing Network (AoD-Net) to directly restore the haze-free result without the needs of estimating the transmission. In [23], a gated fusion network was proposed by learning confidence maps for three inputs processed from the

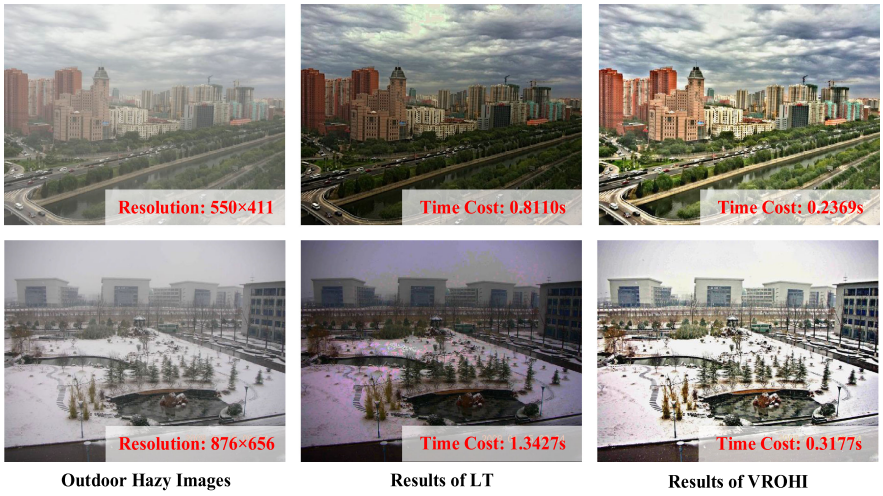

Fig. 1. Comparison between the image dehazing methods using LT [11] and VROHI proposed in this paper (The experiments were all conducted in Matlab2016b with the same configuration environment).

original input. Similar to the second category of dehazing method, this fusion network also lacks the ability to recover the scenes misjudged as the haze-free. Moreover, most deep-learning-based techniques are only trained by synthetic hazy datasets (e.g., NYU Depth dataset [26] and Make 3D dataset [27]), thus they may not uncover the latent contents for the real-world images well, especially for images with heavy haze [15]. Although a semi-supervised learning network [24] has been provided by training both synthetic and real-world hazy images, this method still performs less effective when processing the image suffers from severe haze, as discussed in [24].

In summary, there exist many image dehazing methods in the literature, but most of them are focusing on achieving a high restoration quality and ignoring the processing efficiency, which makes them unsuitable for vision systems that require real-time performance. Therefore, this work aims to develop a highly efficient image dehazing approach while maintaining a good restoration quality. In [28], [29], fast and high-quality hazy remote sensing (RS) data restoration has been made by employing additive haze model (AHM). The key advantage of using AHM to dehaze the high-resolution RS data is due to its simplicity, which leads to significantly reduced computation cost. We assume that AHM may also have the potential to be used to efficiently and effectively restore the outdoor hazy images. However, due to the difference in spectral information between RS data and outdoor images, AHM is not suitable to model the outdoor hazy image and thus current AHM-based methods cannot be directly used on outdoor hazy image restoration.

In this paper, to make use of the simplicity of AHM, AHM is modified into MAHM to make it suitable for outdoor images. Then a highly efficient visibility recovery method for outdoor hazy images, i.e., VROHI, is developed. The core idea of VROHI is to excavate the low-frequency component (LFC) of hazy image, and restore the haze-free result by fully utilizing the latent image feature to constrain the MAHM. In contrast to other dehazing techniques, the proposed VROHI only needs to determine one unknown parameter rather than estimating the transmission to achieve a haze-free result, thereby significantly improving the execution efficiency of haze removal. Fig. 1 illustrates the results comparison between the proposed VROHI and the state-of-the-art dehazing technique LT [11] as an example. As shown in the figure, using VROHI, significant reduction in time consuming is achieved while the quality of the recovered image is also enhanced.

The main contributions of this paper are as follows: The first contribution is the proposed MAHM. In MAHM, the haze thickness map (HTM) is modeled by introducing LFC and two unknown parameters. By accurately extracting the LFC and properly setting these two parameters, one is able to get accurate HTM from the LFC of hazy image, which guarantees subsequent high-quality haze removal. The second one is LFC extraction, which is based on the simple discrete cosine

transform. Its main advantage is that it is able to achieve a similar blur effect in less time compared to traditional filters. The last contribution is global optimization function (GOF), which is modeled by creating a linear function between parameters and imposing saturation prior on MAHM. It enables us to find the only one parameter by making use of whole image rather than local patch, thereby leading to a high-quality restoration.

2. Modified Additive Haze Model

Additive haze model (AHM) proposed in [28] is used to describe remote sensing (RS) images in machine vision and computer graphics. This model is expressed as

$$\mathbf{DN}^i_{\text{observed}}(x, y) = \mathbf{DN}^i(x, y) + \mathbf{HR}^i(x, y), \tag{1}$$

where (x, y) is image coordinate, i is band index, $\mathbf{DN}_{\text{observed}}$ is multi-spectral RS data captured by satellite, $\mathbf{DN}$ is expected surface radiance, and $\mathbf{HR}$ is haze contribution. Unlike the RS data containing both visible bands and additional infrared bands, only three visible RGB bands are included in outdoor images, which means AHM can be further optimized to reduce its complexity.

According to Rayleigh's law [30], the interference of haze depends on the wavelength of light. Since the wavelength variation between the RGB bands for outdoor images is much smaller than that in the multi-bands for RS images, here we assume that the haze contribution to the RGB bands of outdoor images is similar. Consequently, when using AHM to represent RGB bands outdoor hazy images, we propose to use a haze thickness map (HTM) H to replace $\mathbf{HR}^i$ in Eq. (1). This then leads to:

$$\mathbf{I}^c(x, y) = \mathbf{J}^c(x, y) + \mathrm{H}(x, y), \tag{2}$$

where $c \in \{r, g, b\}$ is color channel index, $\mathbf{I}$ is outdoor image contaminated by haze, and $\mathbf{J}$ is haze-free scene radiance.

In [31], Li *et al.* verified that haze is highly related to the illumination component and is concentrated in the low-frequency band of an input image. There exists a quasi-linear relationship between the HTM and the low-frequency component (LFC) of the input image. In this work, by considering the quasi-linear relationship and based on an observation of the haze distribution characteristic of numerous hazy images, gamma correction (GC)[1] is used to relate the HTM with the LFC, i.e.,

$$\mathrm{H}(x, y) = \sigma \cdot (\mathrm{L}(x, y))^{\gamma}, \tag{3}$$

where L is the LFC of the input image, $\gamma \in [0, 1]$ is the GC parameter to adjust the haze distribution, and $\sigma \in [0, 1]$ is a constant related to the haze density. By accurately extracting the LFC and properly setting the values of σ and γ, one is able to get accurate HTM from the LFC of hazy image, which is the premise of subsequent high-quality haze removal.

Combining Eq. (2) and Eq. (3), a modified AHM (MAHM) for outdoor image dehazing can be obtained as

$$\mathbf{J}^c(x, y) = \mathbf{I}^c(x, y) - \sigma \cdot (\mathrm{L}(x, y))^{\gamma}. \tag{4}$$

According to MAHM, the key of image dehazing is to mine LFC and estimate the two constants σ and γ from the input hazy image $\mathbf{I}$, which will be presented in the next section.

[1] Another reason we chose to use GC is because GC has been successfully used to adjust the transmission in [32] while the patterns of HTM and transmission of a hazy image have some similarities.

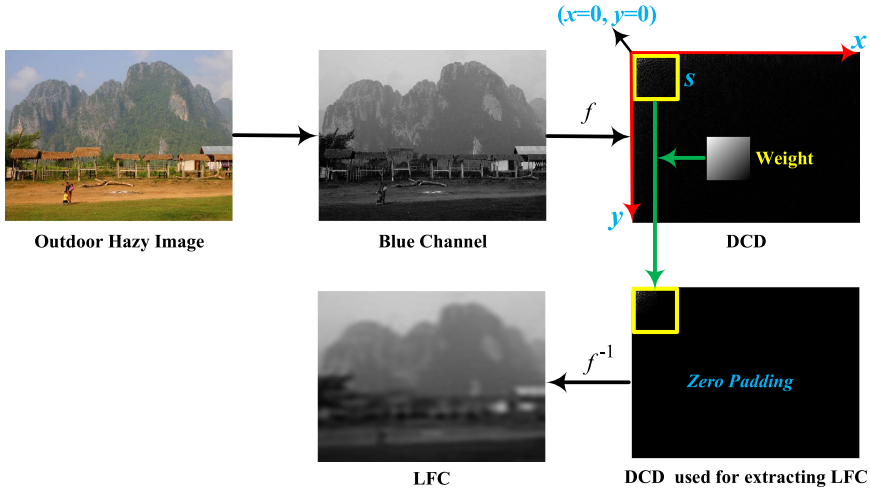

Fig. 2. The working mechanism of Eq. (5).

3. Proposed Technique

In this section, based on the MAHM described in the previous section, a fast visibility recovery method called VROHI is developed for outdoor hazy images. The proposed VROHI consists of two major modules, i.e., extraction of LFC module and global optimization dehazing module.

3.1 Extraction of LFC

According to Rayleighs law [30], the penetration ability of light is proportional to its wavelength. In RGB space, blue channel $\mathbf{I}^b$ corresponds to the smallest wavelength compared to the red and green channels, thus the blue channel is more susceptible to the interference of haze. On this basis, in this work, we attempt to excavate the LFC from $\mathbf{I}^b$ since it is closer to haze distribution. Directly employing image blur tools with edge protection, e.g., guided filter (GF) [33], joint bilateral filter (JBF) [34], and guided total variation (GTV) [35], is the most intuitive way to calculate the LFC. However, these techniques all need complex convolution operators to get the filter weights for each pixel in whole image, which is bound to reduce the computational efficiency of haze removal. In this paper, a low complexity discrete cosine transform based LFC extraction method is proposed. Specifically, this procedure can be expressed by

$$\begin{cases} F = f(\mathbf{I}^b) \\ \mathrm{F_L}(x, y) = \begin{cases} \mathrm{W(x, y)} \cdot \mathrm{F(x, y)}, & 0 \le \mathrm{x} \le \mathrm{s}, 0 \le \mathrm{y} \le \mathrm{s} \\ 0, & \text{else} \end{cases} \\ \mathrm{L} = f^{-1}(\mathrm{F_L}), \end{cases} \tag{5}$$

where $f(\cdot)$ and $f^{-1}(\cdot)$ are the discrete cosine transform (DCT) operator and inverse DCT (IDCT) operator, F is the discrete cosine domain (DCD) of $\mathbf{I}^b$ obtained via DCT, $\mathrm{F_L}$ is the weighted F, s is the size of a square patch selected on F for weighting, and W is the introduced weighting factor.

For clarity, the working mechanism of Eq. (5) is illustrated in Fig. 2. The first step is to obtain the blue channel from input image. Then DCD of $\mathbf{I}^b$ is obtained using DCT. In subsequence, a square patch with the size of s at the upper left corner in the DCD is selected. This is due to the fact that the LFC data are mainly concentrated at the upper left corner in F. Since the data should be more reliable for extracting LFC if it is more closer to the upper left corner [36], to improve the reliability, a weighting function is defined as

$$\mathrm{W}(x, y) = 1 - \frac{x + y}{2 \cdot s}, \tag{6}$$

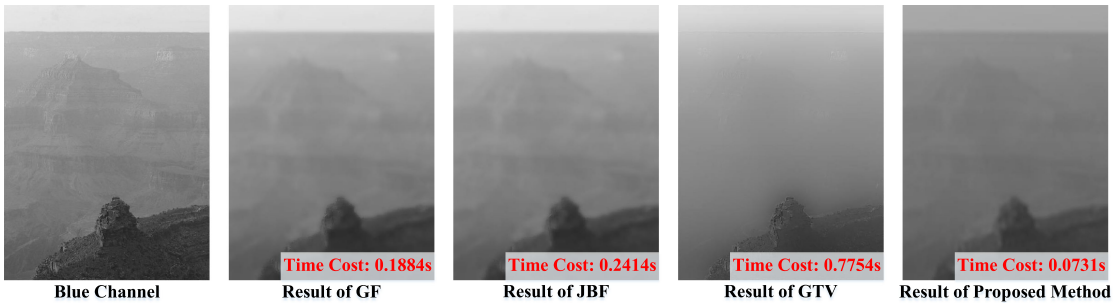

Fig. 3. Comparison of LFC extraction effect between different operators (In this example, the resolution of blue channel is 400 × 600).

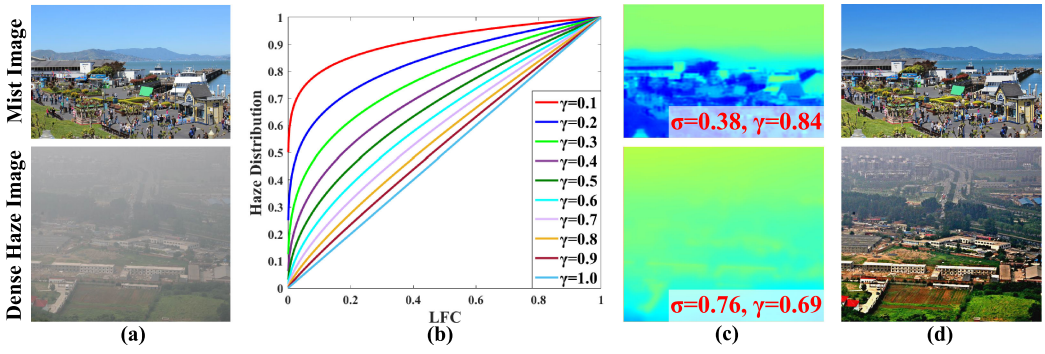

Fig. 4. (a): Outdoor hazy images. (b): Curves of haze distribution with different values of γ. (c): HTMs ($\sigma \cdot \mathrm{L}^{\gamma}$). (d): Recovery Results.

Finally, the LFC is extracted from the weighted F through IDCT. To demonstrate the superiority of the proposed LFC extracting method, Fig. 3 illustrates the LFCs extracted by GF, JBF, GTV, and the proposed method. As observed in the figure, the obtained results are similar but the proposed method consumes much less time.

3.2 Global Optimization Dehazing

In general, mist images usually have sharper haze distribution than images with heavy haze, as shown in Fig. 4(a). In other words, images with high haze density (large σ value) tends to have flatter haze distribution; images with low haze density (small σ value) tends to have sharper haze distribution. Meanwhile, recall the characteristic of GC as shown in Fig. 4(b), i.e., given the input (L in Eq. (3)), the smaller the γ, the flatter the output (H). This leads to a conclusion that there exists an inverse proportional relationship between σ and γ (the larger the σ, the smaller the γ), when using Eq. (3) to model the HTM of a hazy image. There is no doubt that the HTM estimation can be significantly simplified if the relationship between σ and γ can be fitted with a linear equation. Considering that $\gamma \in [0, 1]$ and $\sigma \in [0, 1]$, a following linear function is proposed as

$$\gamma = 1 - \kappa \cdot \sigma, \tag{7}$$

where κ is a parameter introduced to adjust this linear expression to achieve higher accuracy.

Substituting Eq. (5) and Eq. (7) into Eq. (4), the recovery formula can be expressed as

$$\mathbf{J}^{c} = \mathbf{I}^{c} - \sigma \cdot (f^{-1}(\mathrm{F_L}))^{1-\kappa\cdot\sigma}. \tag{8}$$

Algorithm 1: The Proposed VROHI.

Input: Hazy Input **I**

Pre-set parameters:

$s = 100$, $\kappa = 0.4$, $\theta = 0.103$,

Begin:

1. Calculate weight W via Eq. (6).
2. Extract LFC via Eq. (5) using the W.
3. Determine constant σ via Eq. (10) with GSM.
4. Restore haze-free result **J** via Eq. (9).
5. Obtain $\mathbf{J}_e$ by implementing linear stretch on **J**.

Output: Recovery result $\mathbf{J}_e$.

To avoid pixel overflow, the scene radiance $\mathbf{J}^c$ is constrained at the interval [0,1]. Therefore, the expression used for restoring the scene radiance can be rewritten as

$$\begin{aligned}\mathbf{J}^c &= \mathrm{VR}(\kappa, \sigma, \mathbf{I}, f^{-1}(\mathrm{F_L})) \\ &= \min(\max(\mathbf{I}^c - \sigma \cdot (f^{-1}(\mathrm{F_L}))^{1-\kappa\cdot\sigma}, 0), 1),\end{aligned} \tag{9}$$

where VR$(\cdot)$ is the abbreviation of scene radiance restoring function. Note that VR$(\cdot)$ is a function of four parameters, where **I** is the input, $f^{-1}(\mathrm{F_L})$ can be calculated via Eq. (5), κ is the empirical parameter (which will be studied in Section 4), and σ is the only unknown constant related to haze density. To estimate the value of σ accurately, a saturation prior [37] based global optimization function (GOF) is designed as

$$\sigma = \mathrm{argmin}\{\left|\left|\theta - \phi(\mathbf{I}) - \phi(\mathrm{VR}(\kappa, \sigma, \mathbf{I}, \mathrm{f}^{-1}(\mathrm{F_L})))\right|\right|\}, \tag{10}$$

where $\phi(\cdot)$ is saturation operator, θ is average saturation of high-quality image. Once σ is determined via the GOF with golden section method (GSM), the scene radiance can be directly recovered by Eq. (9). However, as previously noted by [7], the dehazed image might look dim, since the radiance is usually not as bright as the atmospheric light. For display, the recovery result is enhanced to be a high dynamic image $\mathbf{J}_e$ by performing a linear contrast stretch [13] on it.

Taking the hazy images in Fig. 4(a) as examples, the HTMs and recovery results using the proposed method are shown in Figs. 4(c) and 4(d), respectively. It can be observed from these results that the estimated HTMs are in line with intuition, and the haze cover in images can be thoroughly removed.

For clarity, the step-by-step procedure of VROHI is outlined in Algorithm 1. Note that the values of the pre-set parameters given in Algorithm 1 are optimized results considering different scenarios. One does not need to re-estimate these parameters when using the VROHI for image dehazing. Also, it is noted that, the steps in this dehazing procedure are all simple operations, which guarantees a high efficiency of the proposed VROHI.

4. Experiments

To evaluate VROHI, each module of VROHI is further assessed by experiments. Then, qualitative and quantitative comparisons are made between the proposed VROHI and other state-of-the-art technologies to demonstrate its superiority. In specific, we tested VROHI on various challenging hazy images and compared the results with those obtained from some well-known algorithms including DCP [7], MSF [18], DehazeNet [20], BCCR [38], NLD [12], CAP [39], DEFADE [18], MSCNN [21], and AoD-Net [22]. Among these methods, DCP, MSF, and DehazeNet are included in the comparison to validate the performance of the proposed global-optimization-based strategy, and the rest algorithms are tested for qualitative and quantitative comparisons of the image dehazing capability.

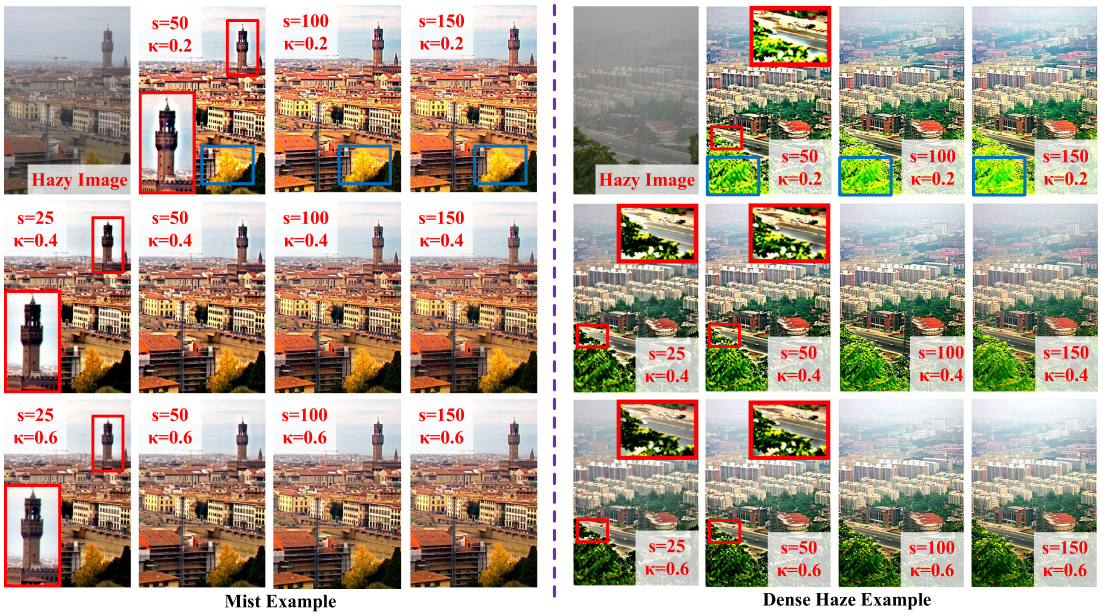

Fig. 5. Image dehazing using VROHI with different combinations of s and κ while θ is fixed at 0.103.

In this work, experiments were conducted by MATLAB2016b on a PC with Intel(R) Core (Tm) i7-8700 CPU@ 3.20 GHz 16.00 GB RAM. Note that the codes of DehazeNet, BCCR, NLD, CAP, DEFADE, and MSCNN are downloaded from the authors' websites. The codes of MSF and DCP are not publicly available, but they are easy to implement.

4.1 Initial Parameter Setup

There are three parameters that need to be initialized in the proposed VROHI, i.e., θ, s, and κ. In this work, the value of θ is selected to be 0.103 according to saturation prior [37]. Only s and κ are new parameters introduced in this work. To find appropriate values for them, the performance test of VROHI on two examples with different combinations of s and κ was conducted, as illustrated in Fig. 5. It can be concluded from this figure that smaller value of s can produce more realistic colors, and the smaller value of κ is able to lead to stronger haze removal ability. However, too small value of s may introduce halo artifact and black effect in the depth jumps (see the zoom-in red patches), and too small value of κ also introduce over-saturation problem in close-range scene (see the blue patches). As a tradeoff, we chose $s = 100$ and $\kappa = 0.4$ in this work since they can achieve the best visual quality. Once the parameters in VROHI are determined, it can be used on all types of images straightforwardly. In following experiments, the recovered results of VROHI are all based on the combination of the determined parameters, as listed in Algorithm 1.

4.2 VROHI Performance Demonstration

4.2.1 Evaluation of Global-Optimization-Based Dehazing: As aforementioned, there are mainly three categories of image algorithms that are proposed to enhance the visibility of images captured in hazy weather. They are the ASM-based, multi-scale-fusion-based, and deep-learning-based methods. Fig. 6 illustrates the processing procedure and the associated running time of the proposed VROHI (global-optimization-based) and three representative techniques, including DCP (ASM-based) [7], MSF (multi-scale-fusion-based) [17], and DehazeNet (deep-learning-based) [20]. As illustrated in Fig. 6, the proposed VROHI only needs to determine one unknown constant while

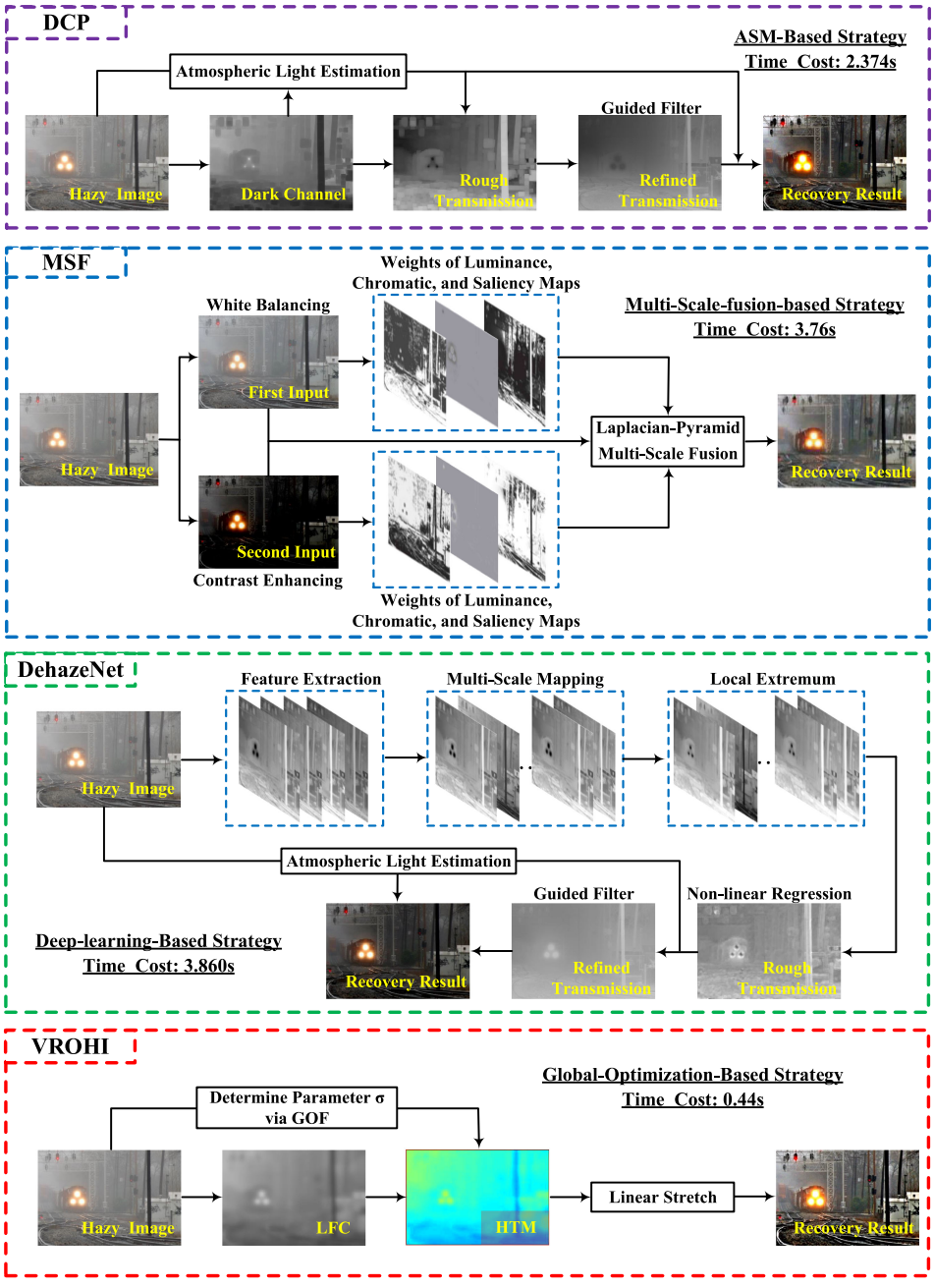

Fig. 6. Overview of image dehazing procedures using DCP, MSF, DehazeNet, and the proposed VROHI.

the other methods need to employ complex tools (such as guided filter and Laplacian-pyramid operator) to realize the haze removal. As a consequence, the proposed global-optimization-based VROHI takes a much shorter time to recover the hazy input.

4.2.2 Evaluation of VROHI on Different Sample Images: After evaluating the global-optimization strategy, the proposed VROHI was then tested on various types of outdoor hazy images obtained from well-known references [7], [15], [40]. Fig. 7 shows the original hazy images, the calculated HTMs, and the corresponding dehazed results to intuitively demonstrate the robustness of VROHI. It can be observed from this figure that VROHI can accurately estimate the HTM and thoroughly

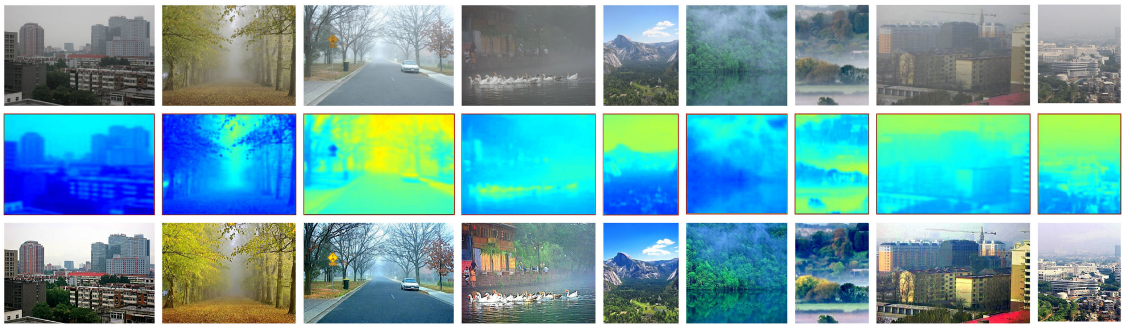

Fig. 7. Visibility recovery result of VROHI on different types of outdoor hazy images. **Top:** Hazy images. **Middle:** Calculated HTMs. **Bottom:** Results recovered via VROHI.

remove the haze from the input image, no matter whether the atmospheric particle distribution is homogeneous or inhomogeneous. Moreover, without introducing any additional post-processing, VROHI still successfully avoids the over-enhancement in the sky regions and the over-saturated in the mist regions.

4.3 Qualitative Comparisons With State-of-The-Art Technologies

4.3.1 Comparison on Challenging Real-World Images: Being able to handle hazy images with complex environment, for example, mist, heavy haze, non-uniform haze, and white-gray scene, is a significant but challenging task for dehazing techniques. Fig. 8 compares the processing results of BCCR (ASM-based) [38], NLD (ASM-based) [12], CAP (ASM-based) [39], DEFADE (multi-scale-fusion-based) [18], MSCNN (deep-learning-based) [21], AoD-Net (deep-learning-based) [22], and the proposed VROHI (global-optimization-based) on six challenging outdoor images.

As shown in Figs. 8(b) and 8(c), both BCCR and NLD can uncover the texture details for all the given images. However, they cannot well handle the regions where the brightness of scene targets is inherently similar to the atmospheric light. In particular, the colors in the recovered rocky areas are completely deviated from the real situation that expected (see the fifth example). For CAP as shown in Fig. 8(d), although it can avoid the above negative problems, its dehazing strength is very weak. This is due to the fact that scattering coefficient used in CAP is simply set as a fixed constant. In Fig. 8(e), DEFADE is able to thoroughly exclude the haze for most given images, but its recovery scenes appear to be darker than they should be. Besides, in the dark regions, the dehazed results using DEFADE suffers from information loss (see the fourth example). As seen in Fig. 8(f) and 8(g), the results obtained via MSCNN and AoD-Net are very visual compelling for mist scenes, whereas they lack the ability to restore to hidden textures for the scenes with heavy haze (see the second example). Moreover, all these comparable methods are not suitable to deal with the image with non-uniform haze (see the third example). The scenes with thick haze in the original picture are still surrounded by some mist in the dehazed results. In comparison, VROHI is able to achieve more realistic haze-free results without these negative visual effects, as shown in Fig. 8(h).

4.3.2 Comparisons on Synthetic Images: Despite the fact that the proposed VROHI is capable of achieving the best recovery results on real-world images, the comparison shown in Fig. 8 might be unfair since it is hard to capture haze-free scenes as the corresponding references of the real-world hazy images. Therefore, we further conducted a comparison between VROHI and state-of-the-art techniques on some sample images from the Realistic Single Image Dehazing (RESIDE) dataset [41], which includes both the hazy images and the corresponding haze-free images. Figs. 9(a)–9(h) show the hazy images and the recovered results based on the synthesized images using BCCR, NLD, CAP, DEFADE, MSCNN, AoD-Net, and the proposed VROHI, respectively. The corresponding ground truth references are given in Fig. 9(i) to facilitate this comparison.

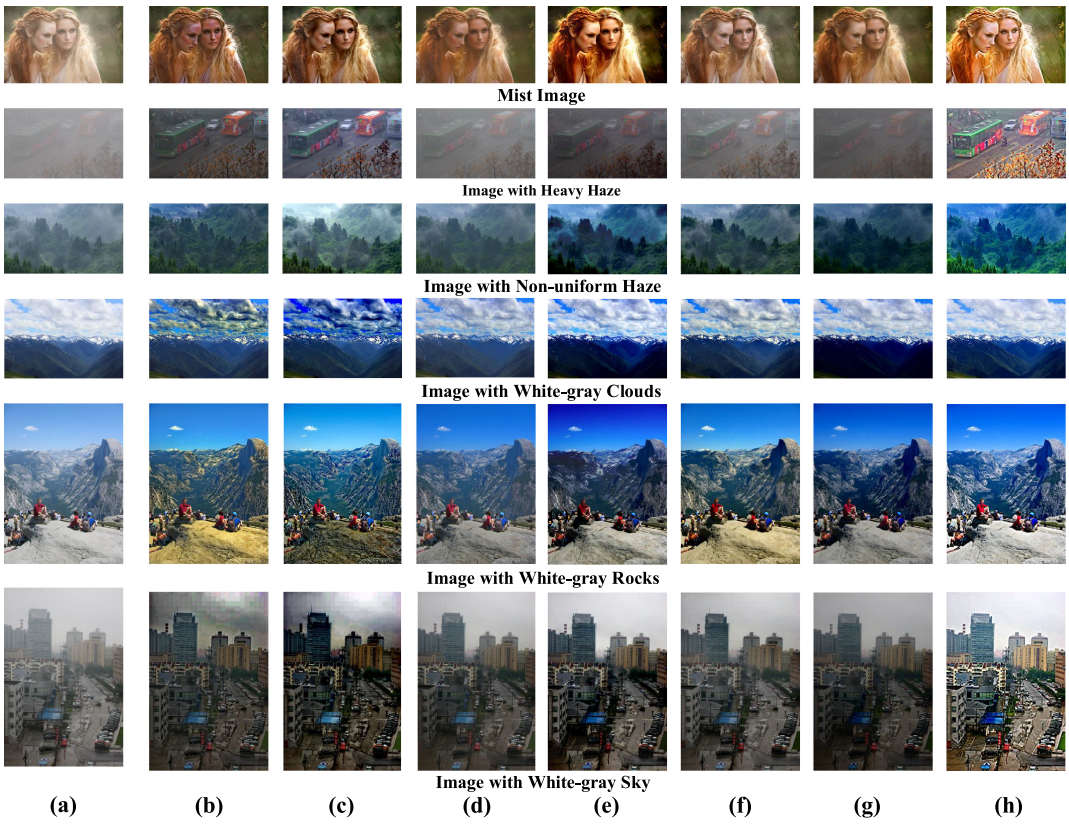

Fig. 8. Qualitative comparison between some state-of-the-art techniques and the proposed VROHI on different kinds of challenging hazy images. (a): Hazy images. (b): BCCR. (c): NLD. (d): CAP. (e): DEFADE. (f): MSCNN. (g): AoD-Net. (h): VROHI.

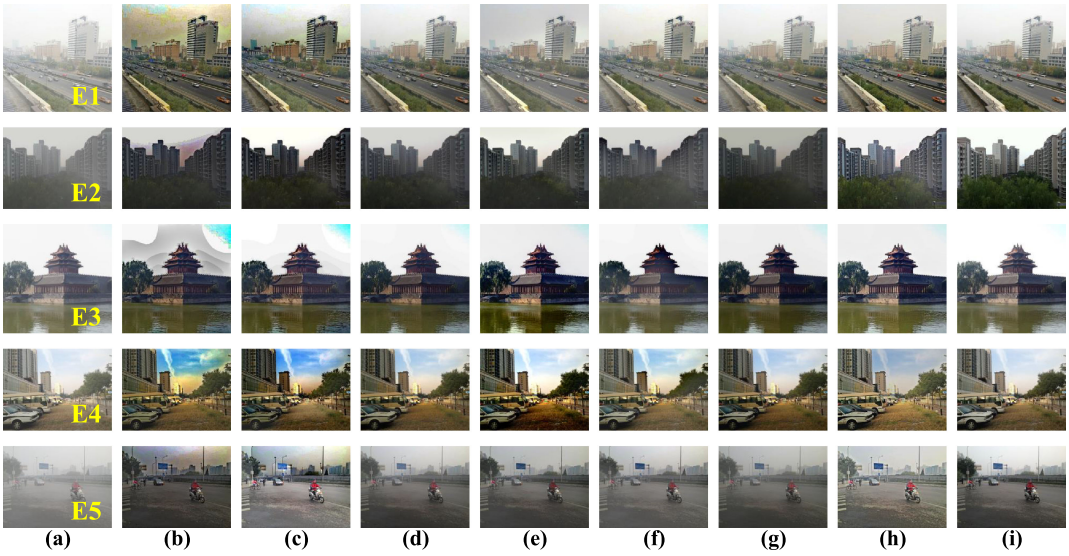

Fig. 9. Qualitative comparison between the proposed VROHI and other state-of-the-art techniques on synthetic images. (a): Hazy Images. (b): BCCR. (c): NLD. (d): CAP. (e): DEFADE. (f): MSCNN. (g): AoD-Net. (h): VROHI. (i): Ground Truth Images.

TABLE 1
Quantitative Comparison of Recovery Images Shown in Fig. 9 Using $\bar{r}$, e, FADE, and PSNR

Metrics	Examples	BCCR	NLD	CAP	DEFADE	MSCNN	AoD-Net	VROHI
$\bar{r}$	$E1$	**3.7767**	2.3792	1.8308	1.5697	1.5930	1.5257	2.3813
	$E2$	1.9603	2.0151	1.6435	1.8490	1.3445	1.2234	**2.4114**
	$E3$	1.7352	1.5047	1.4140	1.8790	0.9982	1.2079	**1.9321**
	$E4$	1.6842	1.5410	1.4206	1.6492	1.0953	1.2081	**2.0003**
	$E5$	2.5712	3.5672	1.6997	1.6405	1.5819	1.4241	**3.2416**
$\bar{r}$ mean value		2.3455	2.2015	1.6017	1.7175	1.3226	1.3178	**2.3933**
e	$E1$	**0.9554**	0.4320	0.3840	0.3511	0.3576	0.3350	0.3978
	$E2$	1.5276	1.8290	1.4496	1.0190	0.6038	1.4896	**1.8510**
	$E3$	0.6079	0.4665	0.4532	0.5688	0.1534	0.5342	**0.6501**
	$E4$	**0.2185**	0.1471	0.1209	0.0721	0.0697	0.0994	0.1414
	$E5$	3.5516	3.6450	3.1755	2.7531	2.2544	3.0072	**3.8907**
e mean value		1.3722	1.3039	1.1166	0.9528	0.6878	1.0931	**1.3862**
FADE	$E1$	**0.3683**	0.5816	0.9374	1.2254	1.1191	1.1733	0.5063
	$E2$	0.6667	0.7886	1.4090	1.1286	1.2724	1.0986	**0.4314**
	$E3$	0.5877	0.5972	0.6752	0.6278	0.8071	1.0885	**0.4755**
	$E4$	0.2732	**0.2562**	0.3568	0.2580	0.5099	0.4158	0.2793
	$E5$	0.5695	0.6592	1.3986	1.3055	1.5745	1.6388	**0.5028**
FADE mean value		0.4931	0.5766	0.9554	0.9091	1.0566	1.0830	**0.4391**
PSNR	$E1$	13.1496	14.9327	24.0319	19.3581	23.7121	25.6268	**26.5301**
	$E2$	13.5973	13.8677	15.5965	15.3929	14.3240	13.9022	**15.5571**
	$E3$	15.1527	18.0433	19.6957	18.7315	22.0421	18.5164	**24.7497**
	$E4$	15.7689	15.3214	22.0249	18.6887	21.0771	21.9374	**22.3663**
	$E5$	13.9008	14.7321	23.0843	19.9370	20.5149	19.6696	**23.7995**
MSE mean value		14.3138	15.3794	20.8794	18.4216	20.3340	19.9304	**23.6005**

As observed in Figs. 9(b) and 9(c), the restored results using BCCR and NLD can clearly indicate the target contour for all the given examples, but the restored colors are generally over-saturated (see the first and fourth examples). In addition, there is also an over-enhancement problem in the sky region (see the third example). As shown in Fig. 9(d), the haze still remains in the second and last examples after the dehazing process of CAP. According to Fig. 9(e), DEFADE achieves a visually pleasing result for most examples, but cannot deal with the fourth example well. As seen in Figs. 9(f) and 9(g), MSCNN and AoD-Net are capable of attaining the haze-free results with vivid color and necessary details for mist scenes. However, haze residue can be found in the second and last examples. Compared to these methods, VROHI is able to moderately uncover the contents and contours from vague scenes. More importantly, VROHI's results do not lead into any negative effects and can maintain the tones of ground truth images, as demonstrated in Fig. 9(h). The success of VROHI lies in the following two aspects. The first one is the effectiveness of MAHM. The most visible manifestation is the estimated HTMs are very consistent with the real haze distributions (see Fig. 7). The second is that the designed GOF is capable of making up the limitation of prior knowledge, thus global optimum results instead of local ones can be obtained.

4.4 Quantitative Comparisons With State-of-The-Art Technologies

Qualitative comparison depends on individual's subjective judgment, which may cause differences in judgment among different viewers. Therefore, widely-recognized metrics including the fog aware density evaluator (FADE) [18], the mean ratio of the gradients at visible edge ($\bar{r}$) [42], the ratio of new visible edges (e) [42], and peak signal-to-noise ratio (PSNR) are used to quantitatively evaluate the proposed VROHI and aforementioned techniques. In general, a smaller FADE indicates a stronger

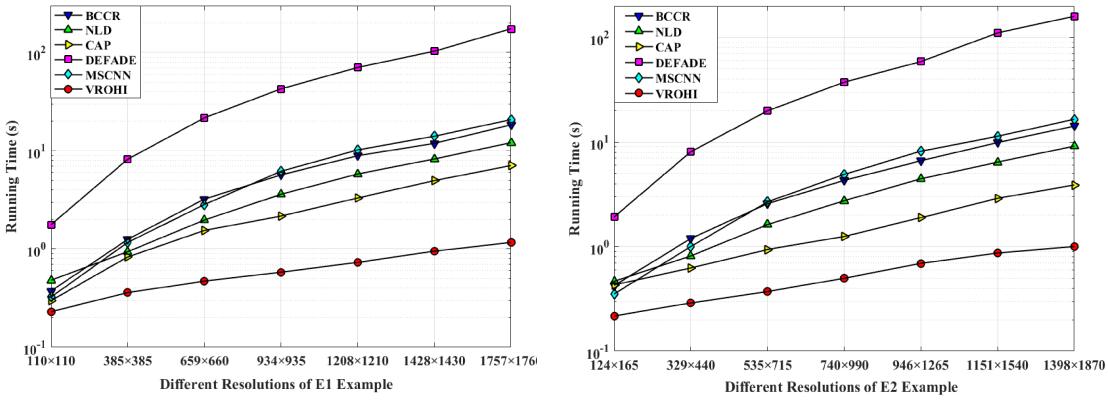

Fig. 10. Comparison of the running time of the states-of-the-art techniques and the proposed VROHI.

restoration ability, larger $\bar{r}$ and e stand for a richer information contained in the recovery results, and a greater PSNR means that the dehazed result is closer to the corresponding real scene.

The values of the assessment metrics on the dehazed results shown in Fig. 9 are summarized in Table 1. It can be concluded from the figure that VROHI achieves the best scores of $\bar{r}$, e, and FADE for the examples E2, E3, and E5. This indicates that VROHI has the ability to restore richer information and remove more haze from single input image. Despite the fact that BCCR and NLD have the better scores of $\bar{r}$, e, and FADE than VROHI for the remaining examples, the images dehazed via these methods appear to be over-enhanced. This might leads to some unreasonable edges, e.g., in the sky regions of the first example. For PSNR, the scores of VROHI are the best compared with other techniques, which means VROHI is able to produce a desirable result similar to ground truth image.

4.5 Efficiency Comparisons

Apart from the restoration quality, the computational complexity is another critical metric for image dehazing technique. Taking the first two hazy images in Fig. 9 as test examples, we further give a comparison of the running time between aforementioned methods and VROHI with different resolutions, as shown in Fig. 10. Please note that AoD-Net is implemented in Pycaffe and the remaining techniques are carried out in Matlab, thus we did not show the running time of AoD-Net for fairness. Due to the employed global-optimization-based strategy, it is not surprising that the proposed VROHI exhibits significantly shorter processing times compared to other techniques. It is more appealing that the time cost curve of VROHI has the smallest slope among those of different algorithms. This illustrates that, as the image resolution increases, the superiority of the proposed VROHI over other techniques, i.e., faster processing, becomes more significant.

5. Conclusion

In this paper, a modified additive haze model (MAHM) is introduced for fast hazy image restoration. Based on this MAHM, a visibility recovery technique for single hazy images called VROHI is further developed. By combining the low-frequency component of hazy image and the saturation prior, VROHI only needs to determine one unknown constant to achieve visibility recovery, and can work well on both mist, heavy haze, inhomogeneous haze, and gray white scene images. In addition, all the operators used in VROHI have lower computational complexity than the tools employed in the state-of-the-art approaches, which makes it a superior candidate for real-time systems. Experiments demonstrate that VROHI achieves an outstanding restoration quality and higher efficiency compared to the state-of-the-art techniques.

References

[1] A. Polesel, G. Ramponi, and V. J. Mathews, "Image enhancement via adaptive unsharp masking," *IEEE Trans. Image Process.*, vol. 9, no. 3, pp. 505–510, Mar. 2000.
[2] L. Teng, F. Xue, and Q. Bai, "Remote sensing image enhancement via edge-preserving multiscale retinex," *IEEE Photon. J.*, vol. 11, no. 2, Apr. 2019, Art. no. 7000310.
[3] J. Kopf *et al.*, "Deep photo: Model-based photograph enhancement and viewing," *ACM Trans. Graph.*, vol. 27, no. 5, pp. 116:1–116:10, Dec. 2008.
[4] X. Li *et al.*, "Pseudo-polarimetric method for dense haze removal," *IEEE Photon. J.*, vol. 11, no. 1, Feb. 2019, Art. no. 6900611.
[5] S. G. Narasimhan and S. K. Nayar, "Contrast restoration of weather degraded images," *IEEE Trans. Pattern Anal. Mach. Intell.*, vol. 25, no. 6, pp. 713–724, Jun. 2003.
[6] M. Reda, Y. Zhao, and J. C. Chan, "Polarization guided autoregressive model for depth recovery," *IEEE Photon. J.*, vol. 9, no. 3, Jun. 2017, Art. no. 6803016.
[7] K. He, J. Sun, and X. Tang, "Single image haze removal using dark channel prior," *IEEE Trans. Pattern Anal. Mach. Intell.*, vol. 33, no. 12, pp. 2341–2353, Dec. 2011.
[8] G. Bi, J. Ren, T. Fu, T. Nie, C. Chen, and N. Zhang, "Image dehazing based on accurate estimation of transmission in the atmospheric scattering model," *IEEE Photon. J.*, vol. 9, no. 4, Aug. 2017, Art. no. 7802918.
[9] Y. Wang, J. Cao, C. Xu, S. Rizvi, K. Li, and Q. Hao, "Fast visibility restoration using a single degradation image in scattering media," *IEEE Photon. J.*, vol. 12, no. 3, Jun. 2020, Art. no. 6100813.
[10] L. He, J. Zhao, N. Zheng, and D. Bi, "Haze removal using the difference- structure-preservation prior," *IEEE Trans. Image Process.*, vol. 26, no. 3, pp. 1063–1075, Mar. 2017.
[11] W. Wang, X. Yuan, X. Wu, and Y. Liu, "Fast image dehazing method based on linear transformation," *IEEE Trans. Multimedia*, vol. 19, no. 6, pp. 1142–1155, Jun. 2017.
[12] D. Berman, T. Treibitz, and S. Avidan, "Non-local image dehazing," in *Proc. IEEE Conf. Comput. Vis. Pattern Recognit.*, Jun. 2016, pp. 1674–1682.
[13] D. Berman, T. Treibitz, and S. Avidan, "Single image dehazing using haze-lines," *IEEE Trans. Pattern Anal. Mach. Intell.*, vol. 42, no. 3, pp. 720–734, Mar. 2020.
[14] Y. Bahat and M. Irani, "Blind dehazing using internal patch recurrence," in *Proc. IEEE Int. Conf. Comput. Photography*, May 2016, pp. 1–9.
[15] M. Ju, C. Ding, D. Zhang, and Y. J. Guo, "BDPK: Bayesian dehazing using prior knowledge," *IEEE Trans. Circuits Syst. Video Technol.*, vol. 29, no. 8, pp. 2349–2362, Aug. 2019.
[16] M. Ju, C. Ding, Y. J. Guo, and D. Zhang, "Idgcp: Image dehazing based on gamma correction prior," *IEEE Trans. Image Process.*, vol. 29, pp. 3104–3118, Dec. 2020.
[17] C. O. Ancuti and C. Ancuti, "Single image dehazing by multi-scale fusion," *IEEE Trans. Image Process.*, vol. 22, no. 8, pp. 3271–3282, Aug. 2013.
[18] L. K. Choi, J. You, and A. C. Bovik, "Referenceless prediction of perceptual fog density and perceptual image defogging," *IEEE Trans. Image Process.*, vol. 24, no. 11, pp. 3888–3901, Nov. 2015.
[19] A. Galdran, "Image dehazing by artificial multiple-exposure image fusion," *Signal Process.*, vol. 149, pp. 135–147, Aug. 2018.
[20] B. Cai, X. Xu, K. Jia, C. Qing, and D. Tao, "Dehazenet: An end-to-end system for single image haze removal," *IEEE Trans. Image Process.*, vol. 25, no. 11, pp. 5187–5198, Nov. 2016.
[21] W. Ren, S. Liu, H. Zhang, J. Pan, X. Cao, and M.-H. Yang, "Single image dehazing via multi-scale convolutional neural networks," in *Proc. Eur. Conf. Comput. Vis.*, 2016, pp. 154–169.
[22] B. Li, X. Peng, Z. Wang, J. Xu, and D. Feng, "Aod-net: All-in-one dehazing network," in *Proc. IEEE Int. Conf. Comput. Vis.*, Oct. 2017, pp. 4780–4788.
[23] W. Ren *et al.*, "Gated fusion network for single image dehazing," in *Proc. IEEE/CVF Conf. Comput. Vis. Pattern Recognit.*, Jun. 2018, pp. 3253–3261.
[24] L. Li *et al.*, "Semi-supervised image dehazing," *IEEE Trans. Image Process.*, vol. 29, pp. 2766–2779, Nov. 2020.
[25] W. Ren *et al.*, "Deep video dehazing with semantic segmentation," *IEEE Trans. Image Process.*, vol. 28, no. 4, pp. 1895–1908, Apr. 2019.
[26] N. Silberman, D. Hoiem, P. Kohli, and R. Fergus, "Indoor segmentation and support inference from rgbd images," in *Proc. Comput. Vis. Eur. Conf. Comput. Vis.*, 2012, pp. 746–760.
[27] A. Saxena, M. Sun, and A. Y. Ng, "Learning 3-d scene structure from a single still image," in *Proc. IEEE 11th Int. Conf. Comput. Vis.*, Oct. 2007, pp. 1–8.
[28] A. Makarau, R. Richter, R. Mller, and P. Reinartz, "Haze detection and removal in remotely sensed multispectral imagery," *IEEE Trans. Geosci. Remote Sens.*, vol. 52, no. 9, pp. 5895–5905, Sep. 2014.
[29] A. Makarau, R. Richter, D. Schlpfer, and P. Reinartz, "Combined haze and cirrus removal for multispectral imagery," *IEEE Geosci. Remote Sens. Lett.*, vol. 13, no. 3, pp. 379–383, Mar. 2016.
[30] E. J. McCartney, *Optics of the Atmosphere: Scattering by Molecules and Particles*. New York, NY, USA: Wiley, 1976.
[31] J. Li, Q. Hu, and M. Ai, "Haze and thin cloud removal via sphere model improved dark channel prior," *IEEE Geosci. Remote Sens. Lett.*, vol. 16, no. 3, pp. 472–476, Mar. 2019.
[32] B. Chen and S. Huang, "Edge collapse-based dehazing algorithm for visibility restoration in real scenes," *J. Display Technol.*, vol. 12, no. 9, pp. 964–970, Sep. 2016.
[33] K. He, J. Sun, and X. Tang, "Guided image filtering," *IEEE Trans. Pattern Anal. Mach. Intell.*, vol. 35, no. 6, pp. 1397–1409, Jun. 2013.
[34] L. Caraffa, J. Tarel, and P. Charbonnier, "The guided bilateral filter: When the joint/cross bilateral filter becomes robust," *IEEE Trans. Image Process.*, vol. 24, no. 4, pp. 1199–1208, Apr. 2015.

[35] M. Ju, D. Zhang, and X. Wang, "Single image dehazing via an improved atmospheric scattering model," *Vis. Comput.*, vol. 33, no. 12, pp. 1613–1625, Dec. 2017.
[36] N. Ahmed, T. Natarajan, and K. R. Rao, "Discrete cosine transform," *IEEE Trans. Comput.*, vol. C-23, no. 1, pp. 90–93, Jan. 1974.
[37] Z. Gu, M. Ju, and D. Zhang, "A single image dehazing method using average saturation prior," *Math. Problems Eng.*, vol. 2017, pp. 1–17, Mar. 2017, Art. no. 6851301.
[38] G. Meng, Y. Wang, J. Duan, S. Xiang, and C. Pan, "Efficient image dehazing with boundary constraint and contextual regularization," in *Proc. IEEE Int. Conf. Comput. Vis.*, Dec. 2013, pp. 617–624.
[39] Q. Zhu, J. Mai, and L. Shao, "A fast single image haze removal algorithm using color attenuation prior," *IEEE Trans. Image Process.*, vol. 24, no. 11, pp. 3522–3533, Nov. 2015.
[40] M. Ju, C. Ding, D. Zhang, and Y. J. Guo, "Gamma-correction-based visibility restoration for single hazy images," *IEEE Signal Process. Lett.*, vol. 25, no. 7, pp. 1084–1088, Jul. 2018.
[41] B. Li *et al.*, "Benchmarking single-image dehazing and beyond," *IEEE Trans. Image Process.*, vol. 28, no. 1, pp. 492–505, Jan. 2019.
[42] N. Hautiere, J.-P. Tarel, D. Aubert, and E. Dumont, "Blind contrast enhancement assessment by gradient ratioing at visible edges," *Image Anal. Stereology*, vol. 27, no. 2, pp. 87–95, May 2011.